

Reanalysis of antiproton production in proton-nucleus and nucleus-nucleus reactions at subthreshold energies*

A. Sibirtsev¹, W. Cassing¹, G.I. Lykasov² and M.V. Rzjanin²

¹Institut für Theoretische Physik, Universität Giessen
D-35392 Giessen, Germany

²Joint Institute for Nuclear Research
141980, Dubna, Moscow Region, Russia

February 9, 2008

Abstract

We reanalyse the production of $p\bar{p}$ pairs in proton-nucleus and nucleus-nucleus collisions employing novel elementary cross sections for baryon-baryon and pion-baryon production channels based on a boson-exchange model. In contrast to previous transport studies performed in the literature the secondary pion induced channel is found to be most important in both p+A and A+A collisions at subthreshold energies. A detailed comparison with the experimental data available indicates that sizeable attractive \bar{p} potentials in the order of - 100 to - 150 MeV at normal nuclear matter density are needed to reproduce the size and shape of the experimental spectra.

*Supported by Forschungszentrum Jülich, BMBF and the Russian Foundation for Fundamental Research

1 Introduction

The production of particles at energies below the free nucleon-nucleon threshold ('sub-threshold production') is one of the most promising observable for hadron selfenergies at high nuclear densities since the particles are produced predominantly during the compressed stage [1, 2, 3, 4]. Antiproton production at energies of a few AGeV is the most extreme subthreshold production process and has been observed in proton-nucleus collisions already a few decades ago [5, 6, 7]. Experiments at the JINR [8] and at the BEVALAC [9, 10] have provided, furthermore, first measurements of subthreshold antiproton production in nucleus-nucleus collisions followed by measurements at KEK [11] and GSI [12, 13] with new detector setups. Various descriptions for these data have been proposed. Based on thermal models it has been suggested that the antiproton yield contains large contributions from $\Delta N \rightarrow \bar{p} + X$, $\Delta\Delta \rightarrow \bar{p} + X$ and $\rho\rho \rightarrow \bar{p}N$ production mechanisms [14, 15, 16]. Other models have attempted to explain these data in terms of multiparticle interactions [17].

Nowadays, the relative strength of the various production channels as well as possible in-medium effects are most effectively controlled by means of transport approaches [18, 19, 20, 21, 22, 23]. First results of a fully relativistic transport calculation for antiproton production including \bar{p} annihilation as well as the change of the quasi-particle properties in the medium have been reported in [21]. There it was found that according to the reduced nucleon mass in the medium the threshold for \bar{p} -production is shifted to lower energy and the antiproton cross section prior to annihilation becomes enhanced substantially as compared to a relativistic cascade calculation where no in-medium effects are incorporated. A variety of transport studies have been performed since then - most of them using the parametrization of the elementary production cross section as proposed by Batko et al. [19] - and confirmed the necessity of attractive \bar{p} potentials, however, with some debate about its actual magnitude [18, 20, 23].

More recently, the question about the elementary \bar{p} production amplitude has been addressed by Lykasov et al. in an effective boson exchange model [24]. Here the production cross section close to threshold follows accurately the 4-body phase-space constraints, but is much lower than the commonly adopted parametrization from [19]. Such a reduced production cross section in baryon-baryon collisions would demand for even stronger attractive \bar{p} potentials if further reactions channels might be neglected. However, as has been found in studies of K^+ and K^- production [25, 26] the secondary pion induced channel might dominate very well such that also the $\pi N \rightarrow Np\bar{p}$ production channel has to be considered.

The paper is outlined as follows: In Section 2 we briefly recall the main ingredients of the relativistic transport approach used for \bar{p} production before [23]. Section 3 is devoted to the calculation of the reaction $\pi N \rightarrow Np\bar{p}$ in a boson exchange model and a presentation of the elementary exclusive and inclusive cross sections. Section 4 contains a detailed comparison of the calculated spectra with experimental data for p+A and A+A collisions with the aim to obtain some closer constraints on the in-medium \bar{p} potential, while a summary on the \bar{p} selfenergies concludes the paper in Section 5.

2 Transport approach for antiproton production and propagation

The phase-space distribution function for the antiprotons $f_{\bar{p}}(x, p_{\bar{p}})$ is assumed to follow an equation of motion equivalent to the transport equation for baryons [27],

$$\left[\frac{\Pi_{\bar{p}}^\mu}{\Pi_{\bar{p}}^0} \partial_\mu + \left(\Pi_{\bar{p}}^\nu F_{\mu\nu}^{\bar{p}} + m_{\bar{p}}^* \left(\partial_\mu^x m_{\bar{p}}^* \right) \right) \partial_{\Pi_{\bar{p}}}^\mu \right] f_{\bar{p}}(x, \Pi_{\bar{p}}) = I_{coll}^{\bar{p}}(x, \Pi_{\bar{p}}) \quad (1)$$

with

$$F_{\bar{p}}^{\mu\nu} = \partial^\mu U_v^{\bar{p}\nu} - \partial^\nu U_v^{\bar{p}\mu} \quad (2)$$

and the mass-shell constraint

$$\left(\Pi_{\bar{p}}^2 - m_{\bar{p}}^{*2} \right) f_{\bar{p}}(x, \Pi_{\bar{p}}) = 0. \quad (3)$$

Since the momentum dependence of the scalar and vector selfenergy of the antiproton are unknown, we assume these quantities to be independent on momentum in Eq. (1), however, to be of different strength as compared to the nucleons,

$$\begin{aligned} U_s^{\bar{p}}(x) &= -g_s^{\bar{p}} \sigma_H(x) \\ U_\mu^{\bar{p}}(x) &= g_v^{\bar{p}} \omega_H(x), \end{aligned} \quad (4)$$

where σ and ω are the scalar and vector meson fields in the nuclear Lagrangian (cf. Ref. [23]). Thus the effective mass and the effective momentum of antiprotons are given by

$$m_{\bar{p}}^* = m + U_s^{\bar{p}}(x) = m - g_s^{\bar{p}} \sigma_H(x) \quad (5)$$

$$\Pi_\mu^{\bar{p}} = p_\mu^{\bar{p}} - U_\mu^{\bar{p}}(x) = p_\mu^{\bar{p}} - g_v^{\bar{p}} \omega_H(x). \quad (6)$$

According to the arguments given before the coupling constants $g_s^{\bar{p}}$ and $g_v^{\bar{p}}$ are treated as free parameters that should be fixed in comparison to data.

2.1 The collision integral

The collision term $I_{coll}^{\bar{p}}$ (r.h.s. of eq. (1)) includes i) a term $I_{elast}^{\bar{p}}$, describing the elastic antiproton-baryon scattering, ii) a term $I_{prod}^{\bar{p}}$, describing the antiproton production by baryon-baryon and meson-baryon collisions, and iii) a term $I_{abs}^{\bar{p}}$ responsible for in-medium \bar{p} -absorption on baryons. The production of $p\bar{p}$ pairs by meson-meson collisions can be neglected in the energy regime of interest here since the invariant energies available are too small. $I_{elast}^{\bar{p}}$ describes elastic baryon-antiproton scattering as well as elastic antiproton-antiproton scattering. While this part of the collision integral $I_{coll}^{\bar{p}}$ can be formulated similarly to the collision term describing bayon-baryon scattering the other terms represent extensions to the conventional collision integral.

The basis for the description of the \bar{p} production by baryon-baryon collisions is the process

$$B + B \rightarrow \bar{p} + p + N + N \equiv 1 + 2 \rightarrow \bar{p} + 3 + 4 + 5, \quad (7)$$

for which the corresponding covariant collision integral reads

$$\begin{aligned}
I_{prod}^{\bar{p}}(x, \Pi_{\bar{p}}) = & \frac{4}{(2\pi)^{11}} \int d^3\Pi_1 d^3\Pi_2 d^3\Pi_3 d^3\Pi_4 d^3\Pi_5 \frac{m_1^* m_2^* m_3^* m_4^* m_5^* m_{\bar{p}}^*}{\Pi_1^0 \Pi_2^0 \Pi_3^0 \Pi_4^0 \Pi_5^0 \Pi_{\bar{p}}^0} \\
& W(\Pi_1^\mu, \Pi_2^\mu \mid \Pi_3^\mu, \Pi_4^\mu, \Pi_5^\mu, \Pi_{\bar{p}}^\mu) \delta^4(p_1^\mu + p_2^\mu - p_3^\mu - p_4^\mu - p_5^\mu - \Pi_{\bar{p}}^\mu) \\
& \{f(x, \Pi_1)f(x, \Pi_2)(1 - f(x, \Pi_3))(1 - f(x, \Pi_4))(1 - f(x, \Pi_5))\}, \quad (8)
\end{aligned}$$

where W is the transition probability for the reaction $\Pi_1 + \Pi_2 \rightarrow \Pi_3 + \Pi_4 + \Pi_5 + \Pi_{\bar{p}}$ in terms of momentum coordinates. We have omitted the Pauli-blocking factor for the antiproton in the final state because the number of antiprotons created during a heavy-ion collision in the subthreshold energy regime is negligible. For the same reason we neglect the effects of the reaction (7) on the phase-space distribution function of the baryons. The production term from πN collisions has a similar structure as Eq. (8) except for the fact that particle 2 denotes a pion and the final state is of 3-body type (with 2 nucleons only) since the 4-momentum of the impinging pion is used entirely for the production of the $p\bar{p}$ pair.

In the collision integral $I_{abs}^{\bar{p}}$ we do not treat all possible annihilation reactions separately but sum up all channels in the inclusive annihilation reaction

$$B + \bar{p} \rightarrow X, \quad (9)$$

where X denotes all possible final states (essentially pions) of the baryon-antiproton annihilation. The corresponding energy and momentum conservation reads

$$p_B^\mu + p_{\bar{p}}^\mu = p_X^\mu, \quad (10)$$

where p_B^μ and $p_{\bar{p}}^\mu$ denote the 4-momenta of the baryon and the antiproton, respectively, and p_X^μ denotes the sum of the 4-momenta of all particles in the final state of the annihilation reaction. Reaction (9) then leads to the collision term

$$\begin{aligned}
I_{abs}^{\bar{p}}(x, \Pi_{\bar{p}}) = & -\frac{4}{(2\pi)^3} \int d^3\Pi_1 d^4\Pi_X \frac{m_1^* m_{\bar{p}}^*}{\Pi_1^0 \Pi_{\bar{p}}^0} \\
& W(\Pi_1^\mu, \Pi_{\bar{p}}^\mu \mid \Pi_X^\mu) \delta^4(p_1^\mu + p_{\bar{p}}^\mu - p_X^\mu) f(x, \Pi_1) f(x, \Pi_{\bar{p}}) \quad (11)
\end{aligned}$$

with $W(\Pi_1^\mu, \Pi_{\bar{p}}^\mu \mid \Pi_X^\mu)$ denoting the transition probability for the reaction (9). Integrating (11) over $d^4\Pi_X$ we obtain

$$I_{abs}^{\bar{p}}(x, \Pi_{\bar{p}}) = -\frac{4}{(2\pi)^3} \int d^3\Pi_1 \frac{m_1^* m_{\bar{p}}^*}{\Pi_1^0 \Pi_{\bar{p}}^0} W(\Pi_1^\mu, \Pi_{\bar{p}}^\mu) f(x, \Pi_1) f(x, \Pi_{\bar{p}}). \quad (12)$$

Here the integration over $d^4\Pi_X$ implies in addition to the integration over all final momentum states of a particular reaction a summation over all possible annihilation channels. Due to this fact $W(\Pi_1^\mu, \Pi_{\bar{p}}^\mu)$ denotes the probability of an antiproton with effective momentum $\Pi_{\bar{p}}^\mu$ to annihilate with a baryon with effective momentum Π_1^μ .

2.2 Numerical implementation

Since the production probability for antiprotons is very small the average time evolution of the nucleus-nucleus is not affected and it is justified to treat the \bar{p} -production perturbatively [2, 3]. Within this approach the \bar{p} invariant differential multiplicity is obtained by summing incoherently over all baryon-baryon and meson-baryon collisions and integrating over all residual degrees of freedom. Assuming the antiproton production to take place via reactions of the type

$$B + B \rightarrow \bar{p} + p + N + N \equiv 1 + 2 \rightarrow \bar{p} + 3 + 4 + 5 \quad (13)$$

$$\pi + B \rightarrow \bar{p} + p + N \equiv 1 + 2 \rightarrow \bar{p} + 3 + 4 \quad (14)$$

(B stands for either nucleon or Δ) the invariant multiplicity as a function of the impact parameter can be written as

$$E_{\bar{p}} \frac{d^3 P(b)}{d^3 \Pi_{\bar{p}}} = \sum_{BB_{coll}} \int d^3 \Pi'_3 d^3 \Pi'_4 d^3 \Pi'_5 \frac{1}{\sigma_{BB}(\sqrt{s})} E'_{\bar{p}} \frac{d^{12} \sigma_{BB \rightarrow \bar{p}+X}(\sqrt{s})}{d^3 \Pi'_3 d^3 \Pi'_4 d^3 \Pi'_5 d^3 \Pi'_{\bar{p}}} \\ (1 - f(x, \Pi'_3)) (1 - f(x, \Pi'_4)) (1 - f(x, \Pi'_5)), \quad (15)$$

$$+ \sum_{\pi B_{coll}} \int d^3 \Pi'_3 d^3 \Pi'_4 \frac{1}{\sigma_{\pi B}(\sqrt{s})} E'_{\bar{p}} \frac{d^9 \sigma_{\pi B \rightarrow \bar{p}+X}(\sqrt{s})}{d^3 \Pi'_3 d^3 \Pi'_4 d^3 \Pi'_{\bar{p}}} \\ (1 - f(x, \Pi'_3)) (1 - f(x, \Pi'_4)), \quad (16)$$

where the quantities Π_i ($i = 1, \dots, 5$) denote the in-medium momenta of the participating baryons. $\Pi_{\bar{p}}$ and $E_{\bar{p}}$ stand for the \bar{p} effective momentum and energy while $s = (\Pi_1^\mu + \Pi_2^\mu)^2$ is the squared invariant energy available in the corresponding baryon-baryon or pion-baryon collision. The first sum of the Eq. (15) is that over all baryon-baryon collisions while the second sum is that over all pion-baryon collisions occurring during the dynamical evolution. An integration over the impact parameter then yields the Lorentz invariant differential production cross section

$$E_{\bar{p}} \frac{d^3 \sigma_{\bar{p}}}{d^3 \Pi_{\bar{p}}} = 2\pi \int db \, b \, E_{\bar{p}} \frac{d^3 P(b)}{d^3 \Pi_{\bar{p}}}. \quad (17)$$

While in free space the threshold for the elementary production reaction is 4 x the nucleon restmass one has to take into account the selfenergies of all participating particles for a production process in the medium. The conservation of energy and momentum has to be guaranteed, i.e. in baryon-baryon reactions

$$p_1^\mu + p_2^\mu = p_3^\mu + p_4^\mu + p_5^\mu + p_{\bar{p}}^\mu, \quad (18)$$

which in terms of effective momenta and effective masses (cf. eqs. (5) and (6)) reads

$$\Pi_1^\mu + U_v^\mu(|\vec{p}_1|, x) + \Pi_2^\mu + U_v^\mu(|\vec{p}_2|, x) = \Pi_3^\mu + U_v^\mu(|\vec{p}_3|, x) + \Pi_4^\mu + \\ U_v^\mu(|\vec{p}_4|, x) + \Pi_5^\mu + U_v^\mu(|\vec{p}_5|, x) + \Pi_{\bar{p}}^\mu + U_v^\mu(x). \quad (19)$$

With the abbreviation

$$\Delta^\mu \equiv U_v^\mu(|\vec{p}_3|, x) + U_v^\mu(|\vec{p}_4|, x) + U_v^\mu(|\vec{p}_5|, x) + U_v^{\bar{p}\mu}(x) - U_v^\mu(|\vec{p}_1|, x) - U_v^\mu(|\vec{p}_2|, x) \quad (20)$$

we obtain in shorthand form

$$\Pi_1^\mu + \Pi_2^\mu = \Pi_3^\mu + \Pi_4^\mu + \Pi_5^\mu + \Pi_{\bar{p}}^\mu + \Delta^\mu. \quad (21)$$

Similar relations are derived for the πN production channels where we assume the pion selfenergy to be identically to zero. This assumption might appear questionable [28, 29, 30], however, it has been found in a couple of studies that the pion dynamics do not indicate strong potentials in the nuclear medium [31, 32].

In order to derive an expression for the differential \bar{p} -multiplicity we assume, as in refs. [17, 19, 33], that the differential elementary \bar{p} production cross section is proportional to the phase-space available for the final state in BB reactions:

$$E_3 E_4 E_5 E_{\bar{p}} \frac{d^{12} \sigma_{BB \rightarrow NNN + \bar{p}}(\sqrt{s})}{d^3 \Pi_3 d^3 \Pi_4 d^3 \Pi_5 d^3 \Pi_{\bar{p}}} = \sigma_{BB \rightarrow NNN + \bar{p}}(\sqrt{s}) \frac{1}{16 R_4(\sqrt{s})} \delta^4(\Pi_1^\mu + \Pi_2^\mu - \Pi_3^\mu - \Pi_4^\mu - \Pi_5^\mu - \Pi_{\bar{p}}^\mu - \Delta^\mu). \quad (22)$$

and

$$E_3 E_4 E_{\bar{p}} \frac{d^9 \sigma_{\pi B \rightarrow NN + \bar{p}}(\sqrt{s})}{d^3 \Pi_3 d^3 \Pi_4 d^3 \Pi_{\bar{p}}} = \sigma_{\pi B \rightarrow NN + \bar{p}}(\sqrt{s}) \frac{1}{8 R_3(\sqrt{s})} \delta^4(\Pi_1^\mu + \Pi_2^\mu - \Pi_3^\mu - \Pi_4^\mu - \Pi_{\bar{p}}^\mu - \Delta_\pi^\mu) \quad (23)$$

in case of πB reactions.

Here, the δ -functions guarantee the energy and momentum conservation and \sqrt{s} is the invariant energy available for the quasi-particles in the initial state. $R_4(\sqrt{s})$ (R_3) is the 4-body (3-body) phase-space integral [34]; it has been included to ensure that the differential cross sections are normalized to the total cross section.

3 Elementary reaction cross sections

3.1 $\pi N \rightarrow \bar{p} X$

Since there are no experimental data on the antiproton production yields in pion induced reactions close to the reaction threshold [35], we have to address to microscopic models in order to obtain closer constraints on this quantity. Here we calculate the cross section of the reaction $\pi N \rightarrow \bar{p} NN$ within the One-Boson-Exchange model (OBE) using the OBE parameters proposed in [36, 37]. Though the OBE results depend on the cut-off parameters Λ_i in the formfactors - which leads to an uncertainty in the \bar{p} production cross section by about a factor of 2 according to our investigations - we here adopt the results of the Bonn-Jülich model [36, 37] for a leading order computation. As in Refs. [24, 38] we will complement the inclusive production of antiprotons at high

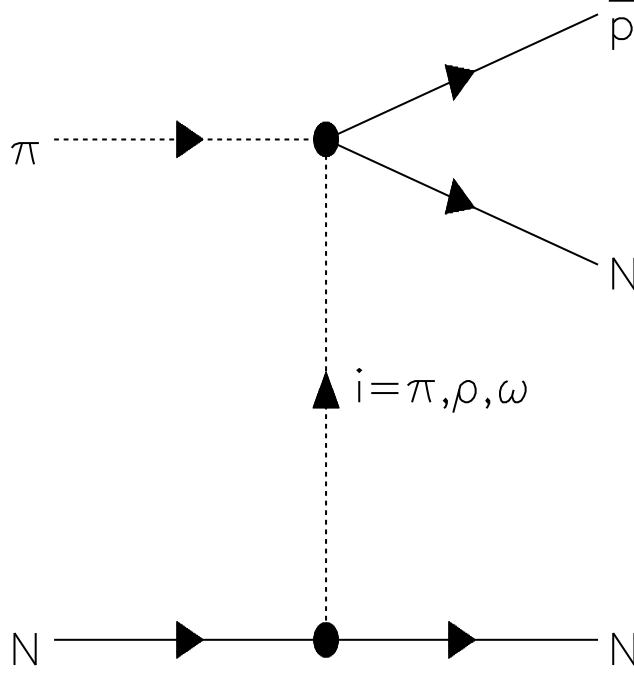


Figure 1: Processes contributing to antiproton production in πN collisions.

energies by calculations within the LUND string model [39] (LSM) to include additionally a multi-hadronic final state with more than two nucleons and an antiproton in the final state.

Fig. 1 illustrates the relevant diagrams for the exclusive reaction $\pi N \rightarrow \bar{p} N N$ which we will compute in the OBE approach. We take into account both pseudoscalar and vector mesons exchanges and express the matrix element as

$$T_{\pi N \rightarrow \bar{p} N N}(t, s) = \sum_i \frac{\bar{u}(p') \Gamma_i u(p) F_i(t)}{t - m_i^2} f_{\pi i \rightarrow \bar{p} N}(s_1), \quad (24)$$

where $f_{\pi i \rightarrow \bar{p} N}(s_1)$ is the amplitude for the process $\pi i \rightarrow \bar{p} N$ and the index i stands for the exchanged π, ρ or ω -meson (cf. Fig. 1), while F_i stands for the corresponding formfactor. Here $u(p)$ and $\bar{u}(p')$ are the spinors of the initial and final nucleons with p, p' being their four-momenta, respectively.

In Eq. (24) s denotes the square of the colliding energy and s_1 is the square of the invariant mass of the $\bar{p} N$ pair, while t is the four momentum transfer from the initial to the final nucleon shown by the lower vertex of the diagram in Fig. 1.

The vertices Γ_i have the following form

$$\Gamma_\pi = g_{\pi N N} \gamma_5, \quad \Gamma_{\omega, \mu} = g_{\omega N N} \gamma_\mu$$

Table 1: The cut-off parameters and coupling constants used in our calculations.

i	$\Lambda_i[\text{GeV}]$	$g_{iNN}^2/4\pi$	f_{iNN}/g_{iNN}
π	0.7	14.4	-
ρ	1.4	0.84	6.1
ω	1.5	20	-

$$\Gamma_{\rho,\mu} = g_{\rho NN} \gamma_\mu + \frac{f_{\rho NN}}{2m} i \sigma_{\mu\nu} k^\nu. \quad (25)$$

where k is the four-momentum of the exchanged ρ -meson.

The ρNN vertex can be rewritten equivalently using the Gordon's relation for the current [36]:

$$\Gamma_{\rho,\mu} = (g_{\rho NN} + f_{\rho NN}) \gamma_\mu - \frac{f_{\rho NN}}{2m} (p + p')_\mu \quad (26)$$

where m is the nucleon mass, $g_{\pi NN}$, $g_{\omega NN}$, $g_{\rho NN}$ are pseudoscalar and vector coupling constants of πNN , ωNN and ρNN interactions, respectively, while $f_{\rho NN}$ stands for the tensor coupling constant. We use the coupling constants from [37, 40, 41]; for completeness they are given in Table 1.

Now the cross section of the reaction $\pi N \rightarrow \bar{p} NN$ can be written as

$$\sigma = \frac{1}{8\pi^2 \lambda(s, m^2, m_\pi^2)} \int_{4m^2}^{(\sqrt{s}-m)^2} ds_1 \lambda^{1/2}(s_1, m_i^2, m_\pi^2) \sigma_{\pi i \rightarrow \bar{p} N}(s_1) \int_{t^-}^{t^+} dt \frac{A_i F_i^2(t)}{(t - m_i^2)^2} \quad (27)$$

where m_i is the mass of the exchanged meson and

$$\lambda(x, y, z) = (x - (\sqrt{y} + \sqrt{z})^2)(x - (\sqrt{y} - \sqrt{z})^2), \quad (28)$$

while

$$t^\pm = 2m^2 - \frac{1}{2s} \left[(s + m^2 - m_\pi^2)(s + m^2 - s_1) \mp \lambda^{1/2}(s, m^2, m_\pi^2) \lambda^{1/2}(s, m^2, s_1) \right]. \quad (29)$$

We use the formfactors in the form

$$F_i(t) = \frac{\Lambda_i^2 - m_i^2}{\Lambda_i^2 - t} \quad (30)$$

with cut-off parameters Λ_i from [37, 41] (cf. Table 1).

Note that $\Lambda_\pi = 0.7$ GeV is taken from [41] and corresponds to the OBE approach of our present paper, while $\Lambda_\pi = 1.3$ GeV is relevant for two-pion exchange corrections as considered in Ref. [37].

In Eq. (27) the functions A_i have the following forms:

$$A_\pi = g_{\pi NN}^2 |t|, \quad A_\omega = g_{\omega NN}^2 |2t + 4m^2|, \quad (31)$$

$$A_\rho = |g_{\rho NN}^2 (2t + 4m^2) + f_{\rho NN}^2 (3t + 5m^2 + \frac{t^2}{4m^2}) + 8t g_{\rho NN} f_{\rho NN}| \quad (32)$$

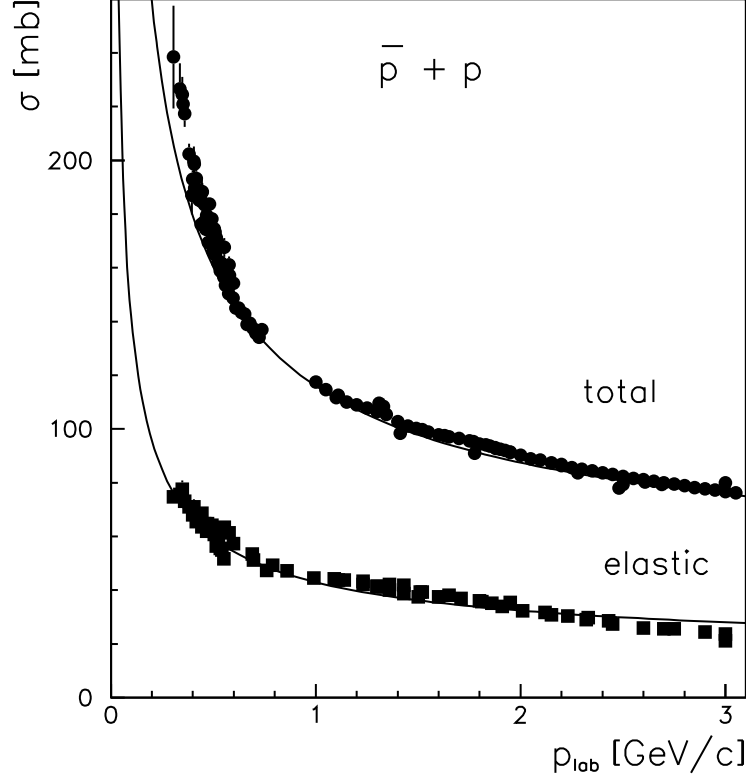


Figure 2: Total and elastic cross sections for $\bar{p}p$ interactions as a function of the laboratory antiproton momentum. The experimental data are from [35] while the lines show the parametrization from the Particle Data Group [42].

In order to calculate $\sigma_{\pi i \rightarrow \bar{p}N}$ we address to available experimental data for the inverse reaction $p\bar{p} \rightarrow \pi\pi, \pi\rho$ as in Ref. [24] which are related by detailed balance as

$$\sigma_{\pi i \rightarrow \bar{p}p}(s_1) = \frac{4}{2J_i + 1} \frac{s_1 - 4m^2}{\lambda(s_1, m_i^2, m_\pi^2)} \sigma_{p\bar{p} \rightarrow \pi i}(s_1) \quad (33)$$

where J_i is the spin of the exchanged meson and $\sigma_{p\bar{p} \rightarrow \pi i}$ is parametrized as [43, 44]

$$\begin{aligned} \sigma_{p\bar{p} \rightarrow \pi i}(s_1) &= C_0 \frac{\lambda^{1/2}(s_1, m_i^2, m_\pi^2)}{2\sqrt{s_1}} \\ &\times \exp \left\{ -A \left[s_1 - (m_\pi + m_i)^2 \right]^{1/2} \right\} \sigma^{tot}(p_{lab}) , \end{aligned} \quad (34)$$

where $C_0 = 9 \text{ mb}(\text{GeV}/c)^{-1}$, $A = 4 \text{ GeV}^{-1}$ and $\sigma^{tot}(p_{lab})$ is the total cross section for $\bar{p}p$ interactions shown in Fig. 2. It can be parametrized by [42]

$$\sigma^{tot}(p_{lab}) = E + Bp_{lab}^n + C \ln^2(p_{lab}) + D \ln(p_{lab}) \quad [mb] \quad (35)$$

where p_{lab} is given in GeV/c and stands for the antiproton momentum in the laboratory system, while the parameters $E = 38.4$, $B = 77.6$, $n = -0.64$, $C = 0.26$, $D = -1.2$ are taken from the Particle Data Group [42].

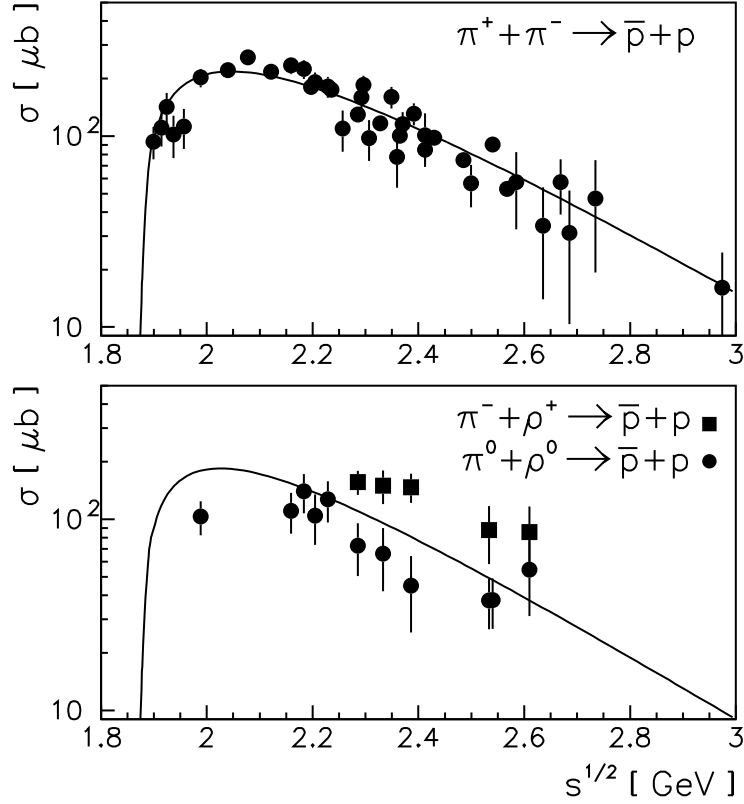


Figure 3: The cross sections for the reactions $\pi + \text{meson} \rightarrow \bar{p}p$. The data are extracted from the experimental cross sections for the inverse reaction [35]; the lines show the parametrization (34).

Fig. 3 shows the experimental data for the reaction $\pi + \text{meson} \rightarrow \bar{p}p$ calculated via detailed balance together with the parametrization (34). In the following calculations we assume that $\sigma_{\pi i \rightarrow \bar{p}N}$ is the same for protons and neutrons and does not depend upon the charge of the exchanged meson.

The cross section of the reaction $\pi^- p \rightarrow pn\bar{p}$ calculated with Eq. (27) is shown in Fig. 4 together with the two available experimental points at higher energy. The solid line indicates the total result, while the dashed, dotted and dashed-dotted lines show the separate contributions from π , ω and ρ -meson exchanges, respectively.

The inclusive cross section for the reaction $\pi p \rightarrow \bar{p}X$ is calculated within the framework of the LSM [39] and is shown in Fig. 5 by triangles. Here the dashed line indicates the results from the OBE model for the exclusive channel. Fig. 5 illustrates a quite reasonable agreement between the results from two different approaches used in our calculations for energies close to threshold.

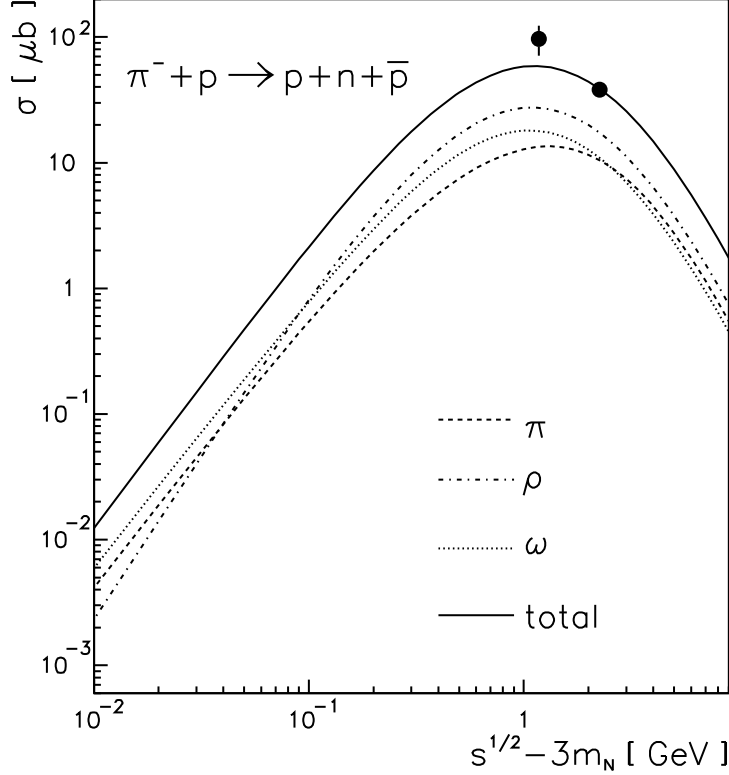


Figure 4: Cross sections for the reactions $\pi^- p \rightarrow pn\bar{p}$. The experimental data are from [35] while the lines indicate our calculations within the One-Boson-Exchange model.

For practical use in transport calculations we parametrize the antiproton production cross section in the form

$$\sigma_{\pi N \rightarrow \bar{p}X} = a \left(\frac{s}{s_0} - 1 \right)^b \left(\frac{s}{s_0} \right)^c \quad (36)$$

with parameters listed in Table. 2. Using the form (36) we also parametrize the cross section for antiproton production from nucleon-nucleon collisions as calculated within the OBE-approach in Ref. [24]. Note that the first term of Eq. (36) reflects the energy dependence of the cross section near the reaction threshold; our final results indicate a phase-space dominance for the antiproton production cross sections both from pion and nucleon induced reactions which supports the ansatz (23) for the multi-differential cross section. It is clearly seen from a comparison of Eq. (36) with parameters b from Table 2.

Fig. 6 shows our parametrizations of the cross sections for antiproton production from πp and pp collisions as a function of the excess energy $\sqrt{s} - \sqrt{s_0}$. The solid circles indicate the experimental data for the reaction $pp \rightarrow \bar{p}X$ [35]. We are not aware of inclusive data for \bar{p} -production by pion induced reactions. Note that the πN channel

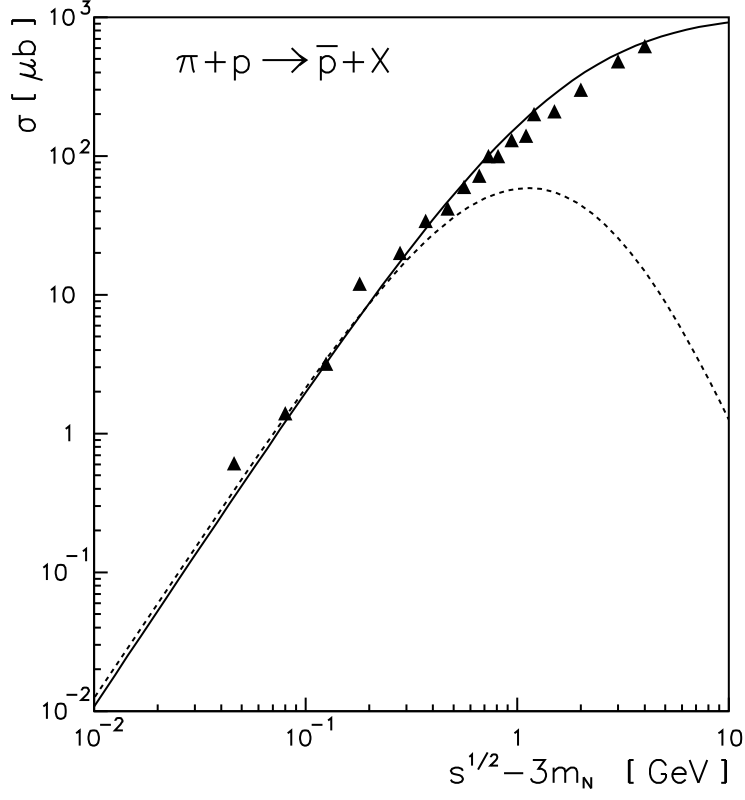


Figure 5: The cross sections for the inclusive antiproton production from pion-nucleon collisions. The triangles show the results from the string model (LSM). The dashed line is our calculation for the exclusive reaction within the OBE approach while the solid line indicates the parametrization (36).

Table 2: The parameters in the approximation (36).

<i>Reaction</i>	s_0	a [mb]	b	c
$\pi N \rightarrow \bar{p}X$	$9 m^2$	1	2.31	2.3
$NN \rightarrow \bar{p}X$	$16 m^2$	0.12	3.5	2.7

above threshold is much larger than the pp channel since it increases with 3-body phase space compared to 4-body phase space for pp . This indicates that the contribution from secondary pion induced reactions to antiproton production in proton-nucleus and heavy-ion collisions might become important or even of leading order.

In the following calculations we assume that the cross sections are the same for the reactions with protons, neutrons and Δ -resonances and for π^+ , π^- and π^0 -mesons.

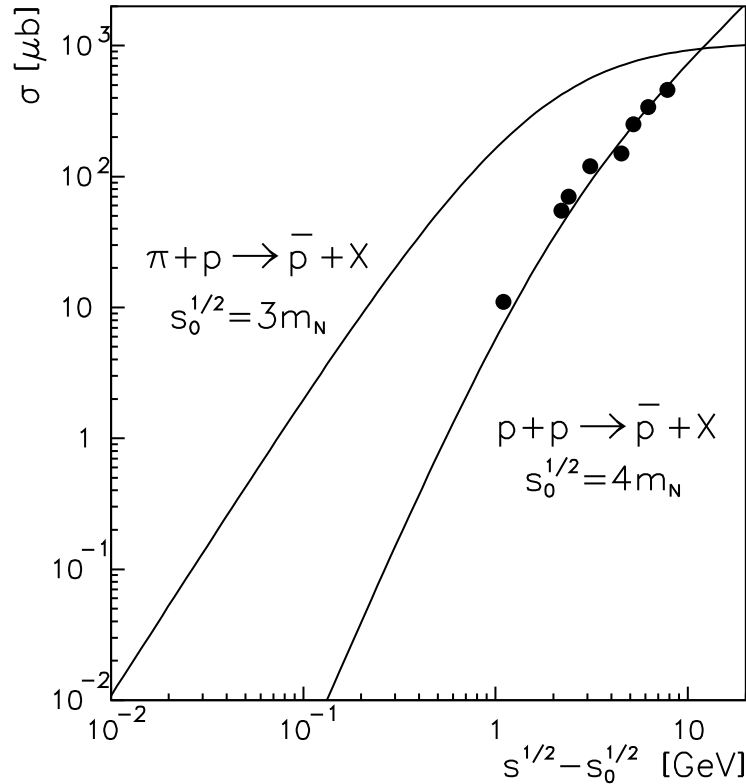


Figure 6: Cross sections of inclusive antiproton production from πp and pp collisions. The circles show the experimental data for the reaction $pp \rightarrow \bar{p}X$ [35] while the lines are the parametrizations (36) of our calculations.

4 Comparison to experimental data

Following the earlier studies on \bar{p} production [22, 23] we now attempt to extract information on the antiproton potentials in the medium by comparing our transport calculations with the available data, i.e. we try to fix the coupling constants $g_s^{\bar{p}}, g_v^{\bar{p}}$ empirically first starting with $g_s^{\bar{p}} = g_v^{\bar{p}} = 0$.

4.1 Proton-nucleus collisions

Detailed experimental studies on antiproton production in $p + A$ collisions at beam energies below the free $NN \rightarrow NNN\bar{p}$ reaction threshold were performed at KEK [11, 45]. Antiprotons with momenta of 1. - 2.5 GeV/c were detected at an emission angle of 5.1° in the laboratory and at beam energies of 3.5, 4, 5 and 12 GeV. The experiments show a very high production cross section at the incident kinetic energy of 3.5 GeV, which is substantially below the free NN threshold of 5.6 GeV.

Here we perform the analysis of antiproton production within the transport model described in Section 2. For the propagation of antiprotons in nuclear matter we account

for both the absorption and elastic scattering. We assume that the elastic cross section is 37% of the total cross section; this simplifying assumption is shown in Fig. 2 by the solid line which reasonably fits the experimental data.

The antiprotons - once produced - strongly interact with the surrounding nuclear matter due to the large $\bar{p}N$ cross section and a large fraction annihilates. Fig. 7 illustrates the nuclear transparency to antiprotons calculated for different targets and defined as the ratio of antiprotons detected asymptotically for $t \rightarrow \infty$ to the total number of antiprotons actually produced in baryon-baryon and pion-baryon collisions.

The histograms in Fig. 7 show our results from the transport model while the solid lines indicate the calculations within the Glauber formalism described in [38]. The Glauber model accounts for the interaction of the initial protons as well as for the annihilation of the antiprotons. However, the rescattering in the nuclear medium is not included in the present version of the Glauber model. Thus the large difference at antiproton momenta $p \geq 2$ GeV/c between the Glauber calculations and the results from the BUU approach illustrated in Fig. 7 is due to rescattering effects, which are most important for heavy nuclei. We find that both calculations agree reasonably well for ^{12}C and ^{64}Cu for which experimental data are available. Both models predict that for heavy nuclei in $p + A$ reactions about 90% of the produced antiprotons annihilate in the target nucleus.

Following the investigations from [22, 23] we study the influence of the antiproton self-energy on the differential \bar{p} -production. In the numerical calculations we adopt the limit $g_v^{\bar{p}} = 0$ as in [23] and vary only the scalar coupling $g_s^{\bar{p}}$ in Eq. (4) in order to obtain the best fit to the experimental data.

Fig. 8 shows the invariant differential cross section for antiproton production in $p + ^{12}C$ collisions at a beam energy of 3.5 GeV and an emission angle of 5° in the laboratory. The experimental data are taken from [45] while the histograms indicate our results calculated with different antiproton potentials (in MeV at saturation density $\rho_0 = 0.16 \text{ fm}^{-3}$). It is clearly seen that without in-medium effects ($U = 0$) we significantly underestimate the production cross section. The agreement becomes better for an attractive antiproton potential of -125 ± 25 MeV at normal nuclear matter density. Figs. 9,10, furthermore, show the experimental data together with our calculations for the reaction $p + C \rightarrow \bar{p}X$ at bombarding energies of 4 and 5 GeV, respectively. Note that at higher energy the data are no longer that sensitive to a variation of the antiproton potential.

The antiproton spectra from $p + Cu$ collisions at bombarding energies of 3.5, 4 and 5 GeV are shown in Fig. 11. The dashed histograms are the results for $U = 0$ MeV, while the solid histograms indicate our calculations with an antiproton potential of $U = -100$ MeV at ρ_0 which almost perfectly fits the experimental data at all energies.

As anticipated before, the πN production channel dominates in $p + A$ reactions at least up to bombarding energies of 6 GeV (cf. Table 3). This finding is fully in line with our studies on K^+ , K^- , ρ , ω and ϕ production for proton-nucleus reactions [38] and results from the fact a) that the Fermi motion can be exploited twice in secondary reactions and b) that the secondary πN collisions have much larger production cross section close to threshold (cf. Fig. 6).

In summary, we get a reasonable fit to the experimental data on antiproton produc-

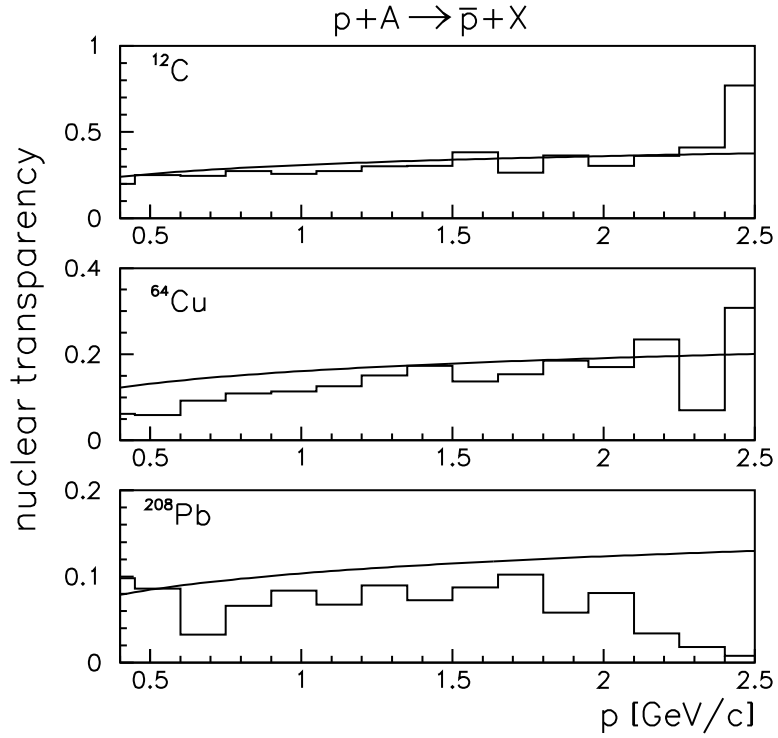


Figure 7: Nuclear transparency for antiprotons produced in $p + A$ reactions. The histograms show calculations within the transport model while the solid lines indicate the results from the Glauber approach in Ref. [38].

Table 3: Cross section σ [nb] for antiproton production in $p + {}^{12}\text{C}$ collisions at bombarding energy T_p calculated for different \bar{p} potentials U [MeV].

T_p [GeV]	Reaction channel	U [MeV]				
		0	-50	-100	-150	-200
5.0	$\pi N \rightarrow \bar{p}$	362	563	824	1210	1670
	$NN \rightarrow \bar{p}$	8.4	20.5	41.7	78.5	138
6.0	$\pi N \rightarrow \bar{p}$	2810	3784	4895	6361	8076
	$NN \rightarrow \bar{p}$	250	384	569	816	1143

tion from proton-nucleus collisions at subthreshold energies with an attractive antiproton potential $U \simeq -125 \pm 25$ MeV at normal nuclear matter density and at antiproton momenta from 1 to 2.5 GeV/c with respect to the nuclear matter at rest.

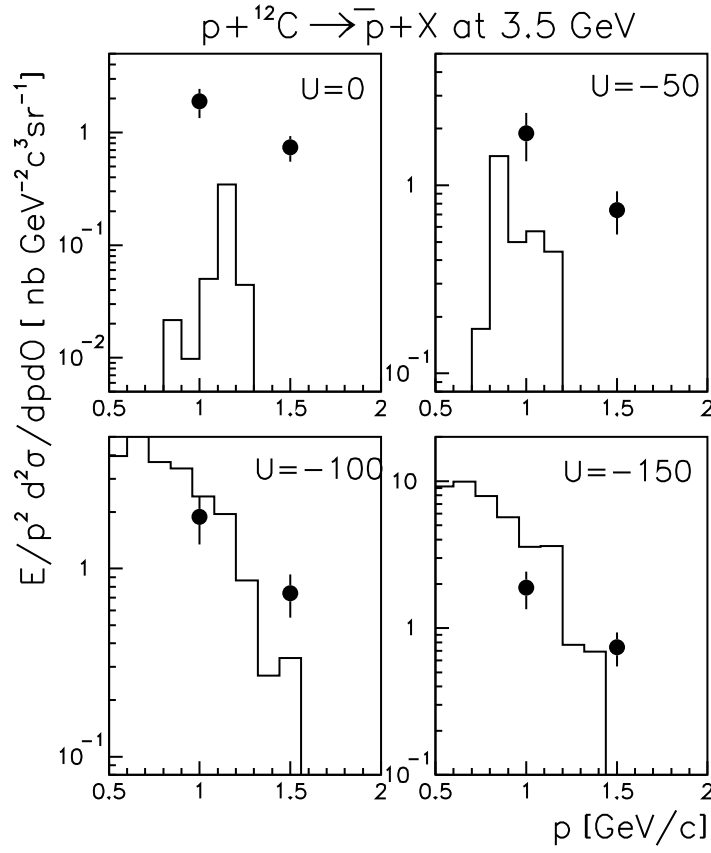


Figure 8: Antiproton spectrum from $p + C$ collisions at a beam energy of 3.5 GeV. The experimental data are from [45] while the histograms indicate our calculations with different antiproton potentials U in MeV.

4.2 Nucleus-nucleus collisions

Experimental studies on antiproton production from heavy-ion collisions at energies below the free NN threshold have been performed at the BEVALAC [33, 46, 47] and at GSI Darmstadt [12, 13].

Whereas in proton-nucleus collisions the antiprotons have quite large momenta relative to the nuclear matter, in heavy-ion reactions the antiprotons have small momenta in the nucleus-nucleus center of mass and are comoving with the expanding 'fireball'. Moreover, heavy-ion reactions probe much higher baryon densities, which influences both the antiproton selfenergy and their final state interactions, i.e. reabsorption and elastic rescattering.

Fig. 12 shows the antiproton spectra from $Si + Si$ collisions at a bombarding energy of 2 A GeV. The experimental data are from [10, 47] while the histograms indicate our calculations for different values of the antiproton potential U (in MeV at ρ_0). In Table 4 we illustrate the relative contribution to antiproton production from NN , ΔN and πN reaction channels for a potential $U = -150$ MeV at ρ_0 . In order to investigate the variation of the cross section with the impact parameter b we also show in Table 4

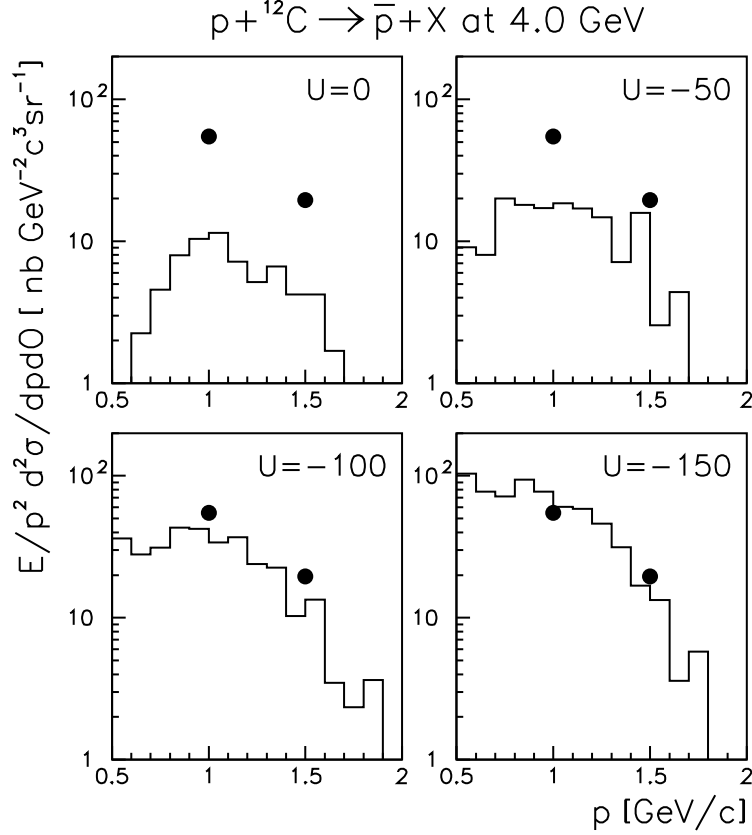


Figure 9: Antiproton spectra from $p + C$ collisions at a beam energy of 4 GeV at $\theta_{lab} = 0^\circ$. The experimental data are from [45] while the histograms indicate our calculations with different antiproton potentials U in MeV at density ρ_0 .

the differential antiproton multiplicity multiplied by the factor $2\pi b$. It becomes clear that the dominant contribution to \bar{p} -production also for $A + A$ collisions stems from the secondary pion induced reactions as in case of $p + A$ collisions. Moreover, the dynamics of antiproton production and propagation show no sizeable difference in the channel decomposition as a function of the centrality of the collision.

Fig. 13 shows the antiproton spectra from $Ni + Ni$ collisions at 1.85 A GeV. The experimental data are taken from [13, 48] and can be reasonably reproduced by our calculations with $U \simeq -125 \pm 25$ MeV at ρ_0 whereas the data are underestimated by about 2 orders of magnitude if no \bar{p} potential is included. Similar statements also hold for the antiproton spectra from $Ne + NaF$ collisions at 1.94 A GeV as shown in Fig. 14 in comparison to the preliminary experimental data from [49].

4.3 Dispersion approach for the antiproton potential

The antiproton potential extracted above empirically from experimental data on \bar{p} -production from $p + A$ and $A + A$ reactions now can be compared with the previous estimates from [22, 23] as well as with the optical potential from a dispersion relation

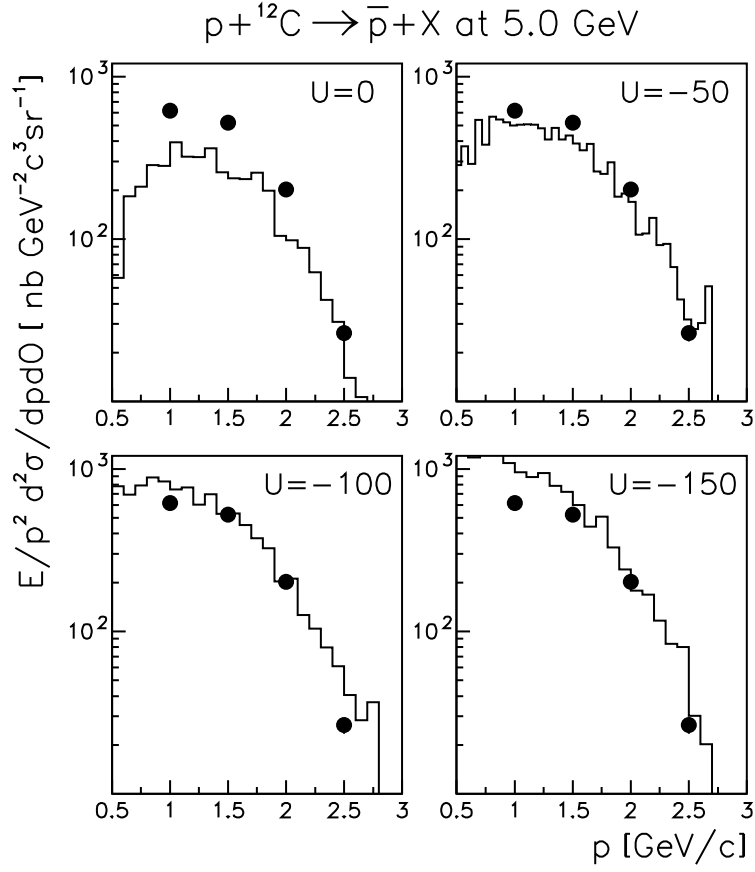


Figure 10: Antiproton spectra from $p + C$ collisions at a beam energy of 5 GeV. The experimental data are from [45] while the histograms indicate our calculations with different antiproton potentials U in MeV at ρ_0 .

Table 4: The differential antiproton multiplicity for $Si + Si$ collisions at 2 A GeV multiplied by the factor $2\pi b$ for an antiproton potential of $U = -150$ MeV at ρ_0 . The decomposition is performed for different impact parameter b and nucleon-nucleon, Δ -nucleon and pion-nucleon reaction channels.

b [fm]	$d\sigma/db$ [nb/fm]		
	NN	ΔN	πN
1	0.64	7.09	22.0
2	1.1	9.5	28.9
3	1.0	7.3	24.5
4	0.67	3.3	4.7
5	0.027	0.63	1.7

approach. In the latter approach the real part of the Schrödinger equivalent potential

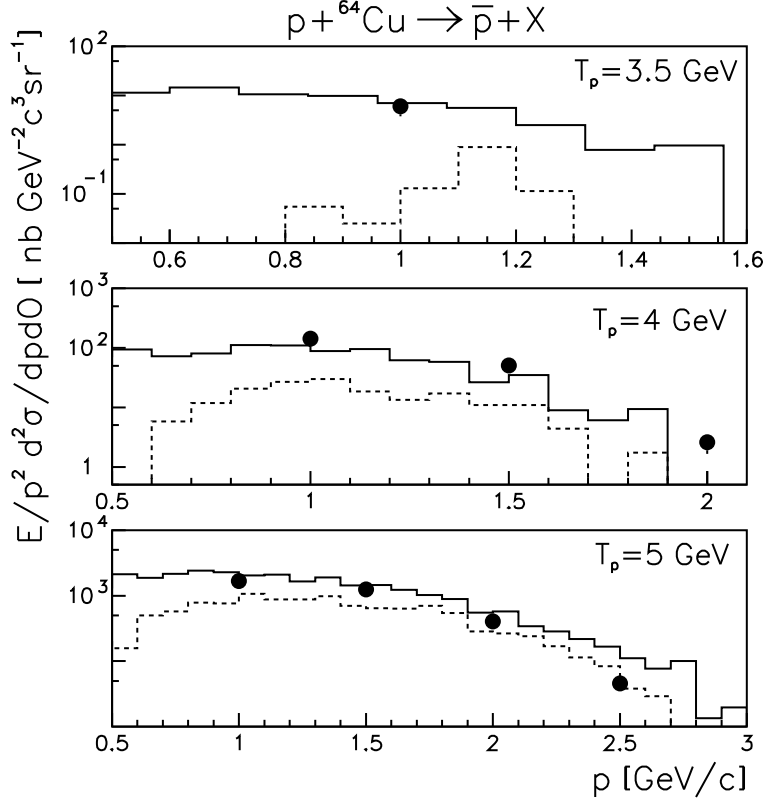


Figure 11: Antiproton spectra from $p + Cu$ collisions at beam energies of 3.5, 4 and 5 GeV. The experimental data are from [45] while the solid histograms show our calculations with an antiproton potential $U = -100$ MeV at ρ_0 ; the dashed histograms indicate our results for $U = 0$.

in the low density approximation is calculated by means of the dispersion relation as

$$U(E, \rho_B) = -\frac{\rho_B}{2\pi} P \int_m^\infty \frac{dE' \sqrt{E'^2 - m^2}}{E' (E - E')} \sigma^{ann}(E') \quad (37)$$

where P stands for the principal value of the integral, σ^{ann} is the annihilation cross section while ρ_B is the baryon density.

The solid line in Fig. 15 shows the antiproton potential calculated by (37) using the parametrization of the annihilation cross section from [14]. We note, that the integral (37) depends sensitively on the parametrization of the annihilation cross section at high energy and that the present result using Ref. [14] should be regarded cautiously. Fig. 15, furthermore, also shows our results extracted from $p + A$ and $A + A$ reactions by the rectangles, which are in a rough agreement with (37) at low momentum.

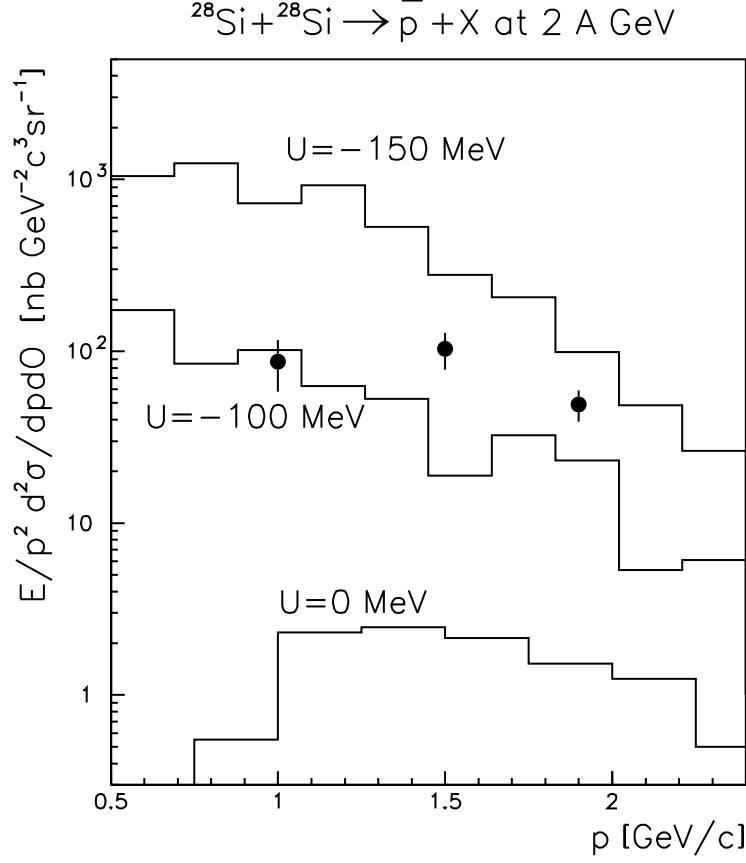


Figure 12: Antiproton spectra from $Si + Si$ collisions at 2.0 A GeV. The experimental data are from [47] while the histograms show our calculations with different antiproton potentials (at ρ_0).

5 Summary

In this study we have evaluated the differential cross section for \bar{p} production for proton-nucleus and nucleus-nucleus reactions in the subthreshold regime by considering on-shell baryon-baryon production channels involving nucleons and Δ 's with their in-medium quasi-particle properties and pion-baryon collisions while treating the \bar{p} propagation and annihilation explicitly. The quasi-particle properties of the nucleons are fixed within our approach by the nuclear saturation properties, the proton-nucleus empirical potential as well as Dirac-Brueckner calculations at higher density as in [22, 23, 32]. Whereas previous studies have neglected the πN production channel and used extrapolations to threshold of the elementary process $p + p \rightarrow \bar{p} + X$, our approach is based on the elementary productions cross section calculated within the OBE approach and within the Lund-string-model at higher energy. These cross sections are in agreement with 3- and 4-body phase-space contrary to the extrapolation from Batko et al. [19] - used so far in almost all studies - which overestimates the pp channel substantially close to threshold.

We have performed a systematic study of p-nucleus and nucleus-nucleus collisions

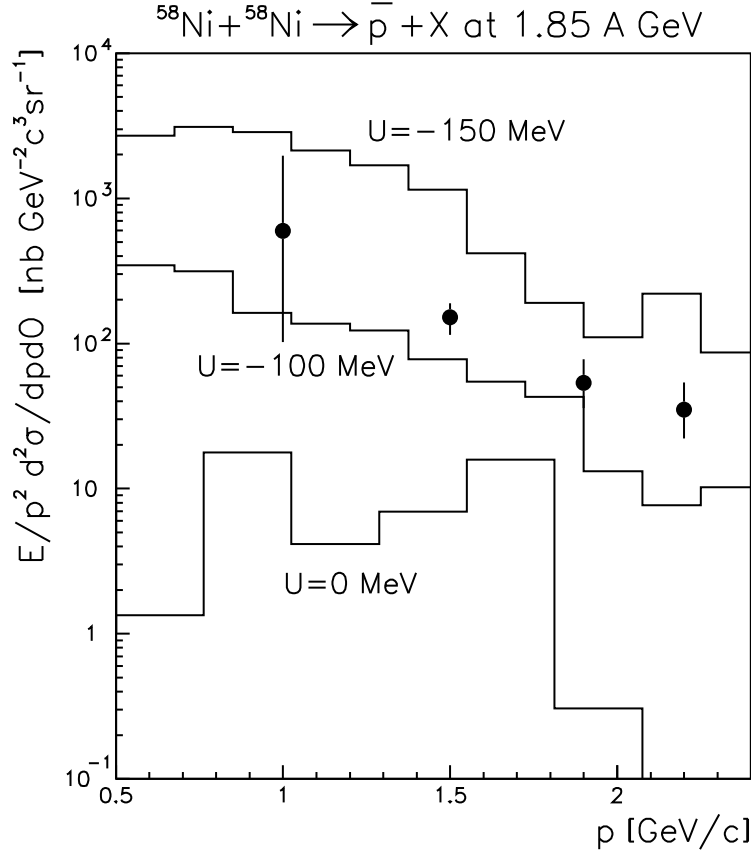


Figure 13: Antiproton spectra from $Ni + Ni$ collisions at 1.85 A GeV at $\theta_{lab} = 0^\circ$. The experimental data are from [13, 48] while the histograms show our calculations with different antiproton potentials U at density $\rho_0 = 0.16 \text{ fm}^{-3}$.

in a broad kinematical regime and compared our numerical results to the data from KEK [11] and GSI [12, 13]. We find a consistent description of all data employing an attractive potential for the antiprotons of about -100 to -150 MeV at ρ_0 which is roughly in line with a dispersive potential extracted from the dominant imaginary part of the antiproton selfenergy due to annihilation. Since the dispersive model itself is known to be valid only at small baryon density and the medium corrections to the annihilation cross section are practically unknown, the agreement between our empirical analysis and the dispersion approach is not considered to be a strong argument. Whereas our novel analysis roughly yields the same \bar{p} potential at low \bar{p} momenta as in Ref. [23] the antiproton potential should be more attractive for momenta above 1 GeV/c (-125 ± 25 MeV) than assumed before.

Our analysis at subthreshold energies, on the other hand, suggests lower antiproton potentials as anticipated from studies at AGS energies [50, 51] where the total antiproton production cross section is no longer that sensitive to its value near the reaction threshold. Here a \bar{p} potential of $\simeq -250$ MeV at ρ_0 is proposed in Refs. [50, 51] for an antiproton at rest with respect to the nuclear matter, whereas an antiproton potential

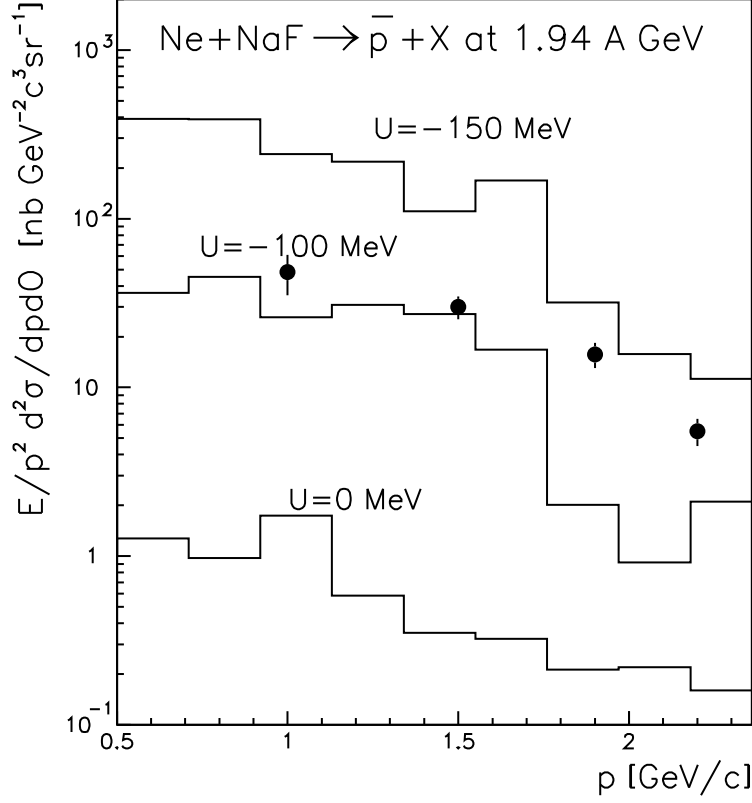


Figure 14: Antiproton spectra from $Ne + NaF$ collisions at 1.94 A GeV. The circles show the preliminary results from [49] while the histograms indicate our calculations for different antiproton potentials (at ρ_0).

of $\simeq -160$ MeV is reported for a \bar{p} momentum of 1 GeV/c [51].

Futhermore, independent from the above uncertainties it has become clear that the \bar{p} production at subthreshold energies is dominated by secondary pion induced reactions as in case of kaons and antikaons [25, 26] since for the new elementary cross sections the baryon-baryon channel is suppressed substantially.

The authors acknowledge valuable discussions with A. Gillitzer and J. Chiba throughout this study and for providing us with their reanalyzed experimental data prior to publication.

References

- [1] G. F. Bertsch and S. das Gupta, Phys. Rep. 160 (1988) 189.
- [2] W. Cassing, V. Metag, U. Mosel, and K. Niita, Phys. Rep. 188 (1990) 363.

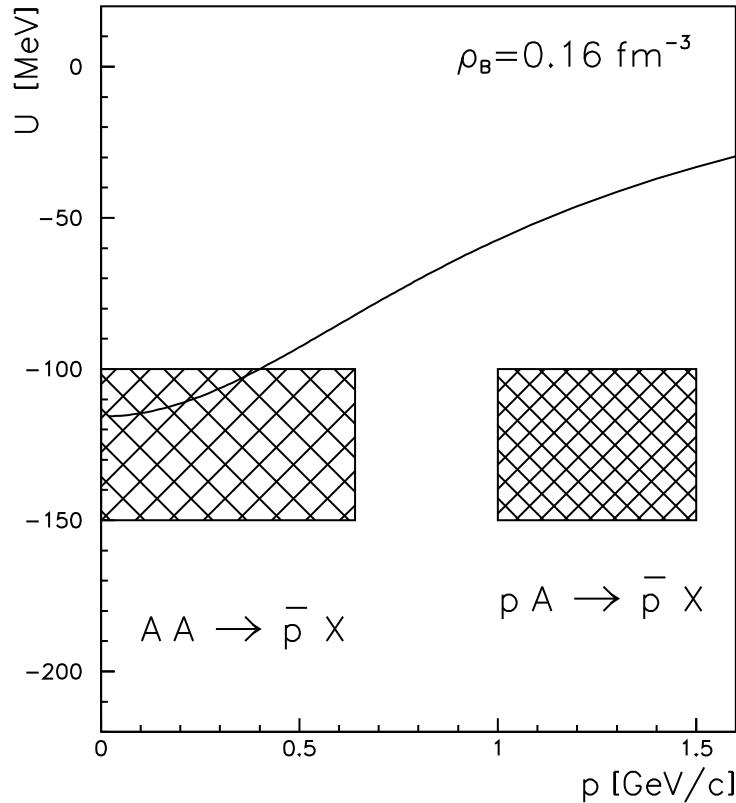


Figure 15: Momentum dependence of the antiproton potential at normal nuclear density ρ_0 . The solid line shows the calculation with the dispersion relation (37) and the annihilation cross section from [14]. The rectangles are from our transport analysis of $p + A$ and $A + A$ reactions, respectively.

- [3] W. Cassing and U. Mosel, Prog. Part. Phys. 25 (1990) 235.
- [4] J. Aichelin, Phys. Rep. 202 (1991) 235
- [5] O. Chamberlain et al., Nuovo Cimento 3 (1956) 447.
- [6] T. Elioff et al., Phys. Rev. 128 (1962) 869.
- [7] D. Dorfman et al., Phys. Rev. Lett. 14 (1965) 995.
- [8] A.A. Baldin et al., JETP Lett. 47 (1988) 137.
- [9] J.B. Carroll et al., Phys. Rev. Lett. 62 (1989) 1829.
- [10] A. Shor, V. Perez-Mendez and K. Ganezer, Phys. Rev. Lett. 63 (1989) 2192.
- [11] J. Chiba et al., Nucl. Phys. A553 (1993) 771c.
- [12] A. Schröter et al., Nucl. Phys. A553 (1993) 775c.

- [13] A. Schröter et al., Z. Phys. A350 (1994) 101.
- [14] P. Koch and C. B. Dover, Phys. Rev. C40 (1989) 145.
- [15] C.M. Ko and X.Ge, Phys. Lett. B205 (1988) 195.
- [16] C.M. Ko and L.H. Xia, Phys. Rev. C40 (1989) R1118.
- [17] P. Danielewicz, Phys. Rev. C42 (1990) 1564
- [18] G.Q. Li, C.M. Ko, X.S. Fang and Y.M. Zheng, Phys. Rev. C49 (1994) 1139.
- [19] G. Batko, W. Cassing, U. Mosel, K. Niita and Gy. Wolf, Phys. Lett. B256 (1991) 331.
- [20] S.W. Huang, G.Q. Li, T. Maruyama and Amand Faessler, Nucl. Phys. A547 (1992) 653.
- [21] W. Cassing, A. Lang, S. Teis and K. Weber, Nucl. Phys. A545 (1992) 123c
- [22] S. Teis, W. Cassing, T. Maruyama and U. Mosel, Phys. Lett. B319 (1993) 47.
- [23] S. Teis, W. Cassing, T. Maruyama and U. Mosel, Phys. Rev. C50 (1994) 388.
- [24] G.I. Lykasov, M.V. Rzjanin and W. Cassing, Phys. Lett. B387 (1996) 691.
- [25] W. Cassing, E.L. Bratkovskaya, U. Mosel, S. Teis and A. Sibirtsev, Nucl. Phys. A614 (1997) 415.
- [26] E.L. Bratkovskaya, W. Cassing and U. Mosel, Nucl. Phys. A622 (1997) 593.
- [27] K. Weber, B. Blättel, W. Cassing, H.C. Dönges, V. Koch, A. Lang and U. Mosel, Nucl. Phys. A539 (1992) 713.
- [28] T. Yamazaki et al., Z. Phys. A 355 (1996) 219.
- [29] T. Yamazaki et al., submitted to Phys. Lett. B.
- [30] T. Waas, R. Brockmann and W. Weise, Phys. Lett. B 405 (1997) 215.
- [31] W. Ehehalt, W. Cassing, A. Engel, U. Mosel and Gy. Wolf, Phys. Lett. B298 (1993) 31.
- [32] W. Ehehalt and W. Cassing, Nucl. Phys. A602 (1996) 449.
- [33] A. Shor, V. Perez-Mendez and K. Ganezer, Nucl. Phys. A514 (1990) 717.
- [34] E. Byckling and K. Kajantie, *Particle Kinematics* (John Wiley and Sons, London, 1973).
- [35] Landolt-Börnstein, New Series, vol. I/12, ed. H. Schopper, Springer, Berlin (1988)
- [36] K. Holinde, Phys. Rep. 68 (1981) 121.

- [37] R. Machleidt, K. Holinde and Ch. Elster, Phys. Rep. 149 (1987) 1.
- [38] A. Sibirtsev, W. Cassing and U. Mosel, Z. Phys. A 358 (1997) 357.
- [39] B. Nilsson-Almqvist and E. Stenlund, Comp. Phys. Comm. 43 (1987) 387.
- [40] J.M. Laget, F. Wellers and J.F. Lecomte, Phys. Lett. B257 (1991) 254.
- [41] M. Brack, D.O. Riska and W. Weise, Nucl. Phys. A287 (1977) 425.
- [42] Particle Data Group, Phys. Rev. D50 (1994) 1335.
- [43] C.J. Hammer, Il Nuovo Cim. 12A (1972) 162.
- [44] J. Vandermeulen, Z. Phys. C37 (1988) 563.
- [45] J. Chiba, private communication.
- [46] J.B. Carrol et al., Phys. Rev. Lett. 62 (1989) 1829.
- [47] A. Shor et al., Phys. Rev. Lett. 63 (1989) 2192
- [48] A. Gillitzer, private communication.
- [49] P. Kienle and A. Gillitzer, Proc. Int. Conf. Nucl. Phys. at the Turn of the Millennium, Wilderness, South Africa, 1996, p. 249.
- [50] V. Koch, G.E. Brown and C.M. Ko, Phys. Lett. B 256 (1991) 29.
- [51] C. Spieles, M. Bleicher, A. Jahns, R. Mattiello, H. Sorge, H. Stöcker and W. Greiner, Phys. Rev. C 53 (1996) 2011.